Scientific Research Publishing

Journal of Computer and Communications, 2026, 14(1), 158-169
https://www.scirp.org/journal/jcc
ISSN Online: 2327-5227
ISSN Print: 2327-5219

An Advanced Antenna Architectures for China's Future Geostationary Microwave Radiometry

Lichang Zhang[1], Hualong Hu[1], Xiangqin Li[2], Hao Wang[1], Yongjian Yang[2], Qianxun Xiao*

[1]Shanghai Institute of Satellite Engineering, Shanghai, China
[2]Shanghai Aerospace Electronic Technology Institute, Shanghai, China
Email: *q_q_zone@163.com

How to cite this paper: Zhang, L.C., Hu, H.L., Li, X.Q., Wang, H., Yang, Y.J. and Xiao, Q.X. (2026) An Advanced Antenna Architectures for China's Future Geostationary Microwave Radiometry. *Journal of Computer and Communications*, **14**, 158-169.
https://doi.org/10.4236/jcc.2026.141010

Received: December 25, 2025
Accepted: January 27, 2026
Published: January 30, 2026

Abstract

This paper presents the design of a 5 m aperture three-reflector offset-fed Cassegrain antenna. A set of rotating fast-scanning mirrors installed at the feed aperture enables one-dimensional rapid scanning observation from geostationary orbit. To meet launch vehicle envelope constraints, the 5 m primary reflector employs a segmented construction, and the secondary reflector utilizes a folded-optics design based on its virtual focus. The antenna's radiation performance was simulated and tested, demonstrating a total main beam efficiency better than 90% and a radiation pattern uncertainty between semi-physical simulation and measurement of better than 1%.

Keywords

Geostationary Orbit, Cassegrain Antenna, Radiation Performance Test, Radiation Pattern

1. Introduction

High-temporal-resolution and high-precision monitoring of severe weather events, such as typhoons, rainstorms, and strong convection, constitutes a core challenge in enhancing the accuracy of weather forecasting. Based on the current utilization of data from microwave temperature and humidity sounders onboard polar-orbiting satellites, microwave atmospheric sounders have proven capable of effectively revealing the internal atmospheric thermal structure of weather systems like typhoons and rainstorms. This plays a significant role in improving the standards of both general weather forecasting and Numerical Weather Prediction (NWP) [1]. However, despite the advantages of multi-channel capabilities and high resolution offered by polar-orbiting meteorological satellites, their long revisit periods fail to meet the application requirements for the real-time monitoring of severe

weather [2]. Therefore, the development of geostationary microwave remote sensing technology—enabling all-day, all-weather, and high-frequency detection of three-dimensional cloud and precipitation structures—permits minute-scale observations of the evolution of typhoon eyes, eyewalls, spiral rainbands, and basin-scale precipitation cloud clusters. This technology fills the global gap in high-frequency, three-dimensional atmospheric profiling within cloudy and rainy regions, holding revolutionary significance for enhancing the timeliness of rainstorm warnings and the accuracy of typhoon track prediction.

Unlike polar-orbiting radiometers, geostationary microwave radiometers require two-dimensional beam scanning. Due to the requirement for high temporal resolution observation of specific regions within the sub-satellite disk, traditional line-by-line mechanical scanning would necessitate extremely high motion speeds for the entire payload. This would generate torque disturbances exceeding the magnitude of 10 N·m, rendering platform attitude compensation impossible. Furthermore, given the high orbital altitude, the radiometer's detection frequency bands must extend into the millimeter and sub-millimeter wave ranges to achieve adequate spatial resolution. If an electronic scanning array approach were adopted, it would be difficult to maintain phase consistency among the array elements; this would severely compromise detection accuracy and fail to meet the requirements for quantitative applications. Additionally, the instrument requires a wide field of view while being constrained within the satellite's limited spatial envelope, making it difficult to balance the number of frequency bands with physical layout limitations [3]. The main technical specifications of the geostationary microwave radiometer are as follows.

1) Operating Frequency Bands: 50 - 60, 89, 118, 166, 183 GHz;
2) Spatial Resolution: 50 km (at nadir);
3) Scanning Disturbance Torque: ≤0.2 N·m;
4) Main Beam Efficiency: ≥90%;
5) Sensitivity: 0.5 - 1.5 K;
6) Calibration Accuracy: ≤1.5 K.

Based on the analysis and technical specifications outlined above, it is evident that the development of geostationary microwave radiometers requires overcoming critical challenges related to spatial resolution, beam scanning, multi-band multiplexing, and system calibration. Only by addressing these issues does the engineering implementation of geostationary microwave remote sensing payloads become feasible.

To date, all on-orbit microwave remote sensing payloads are mounted on Low Earth Orbit (LEO) satellite platforms. In the context of high-orbit real aperture microwave remote sensing systems, neither the U.S. GEM project (featuring a 2 m aperture antenna) nor the European GOMAS project (featuring a 3 m aperture antenna) successfully overcame the bottlenecks associated with spaceborne [4]. Through special research initiatives during the "13th Five-Year Plan", China successfully developed a ground-based principle prototype of a geostationary micro-

wave radiometer. This development pioneered a 5m-aperture compact offset Cassegrain antenna system, and the project has currently entered the engineering development phase.

To address the spatial resolution and beam scanning requirements for meteorological detection by geostationary microwave radiometers, this paper presents a design for a 5 m aperture offset Cassegrain antenna. By employing a segmented primary reflector and virtual focal point mirroring of the sub-reflector to overcome launch envelope constraints, and by integrating a rotating fast-scanning mirror group at the feed aperture [5], the design achieves one-dimensional fast-scanning capability on a GEO platform. This paper provides a detailed elaboration of the antenna's electrical performance, scanning method, and structural design. Furthermore, a comparative analysis between semi-physical simulations and near-field tests of the antenna pattern is conducted, providing theoretical support and a data foundation for the subsequent on-orbit application of geostationary microwave radiometers.

2. Antenna System Design

2.1. Antenna Design Requirements

The core function of the geostationary microwave radiometer is to precisely observe the radiometric brightness temperature of various regions on Earth. Since the amplitude of the brightness temperature noise signal is extremely low, the radiometer requires an antenna system with low sidelobes and high main beam efficiency to meet detection accuracy requirements [6]. The reflector antenna is a widely adopted antenna type; by optimizing its edge illumination level, a main beam efficiency exceeding 90% can be achieved in the millimeter-wave band. The main electrical specifications of the reflector antenna are shown in **Table 1**, including polarization, half-power beamwidth (far-field), main beam efficiency, and beam pointing accuracy.

Table 1. Antenna main electrical specifications

Center Frequency (GHz)	54	89	118.75	165.5	183.31
Operating Bandwidth (GHz)	8	2	12	3	16
Polarization	H	V	H	V	H
Beamwidth	≤0.097˚	≤0.062˚	≤0.062˚	≤0.040˚	≤0.040˚
Beam Pointing	≤0.0097˚	≤0.0062˚	≤0.0062˚	≤0.0040˚	≤0.0040˚
Main Beam Efficiency			≥90%		
Consistency between Simulation and Measurement			≤1%		

The geostationary microwave radiometer employs a two-dimensional scanning scheme. One dimension of scanning is achieved through the attitude maneuvering of the satellite platform. The other dimension is realized by utilizing the off-focus

characteristic of the reflector antenna feed; specifically, a set of rotating fast-scanning mirrors is added at the feed aperture. The rotation of these mirrors enables the feed to scan along a circumference. The system is designed with a beam scanning mode where the beam deviates 0.55˚ from the nadir, covering a ground scanning observation sector of 110˚ within each rotational scanning cycle. The schematic of the antenna scanning detection is shown in **Figure 1**.

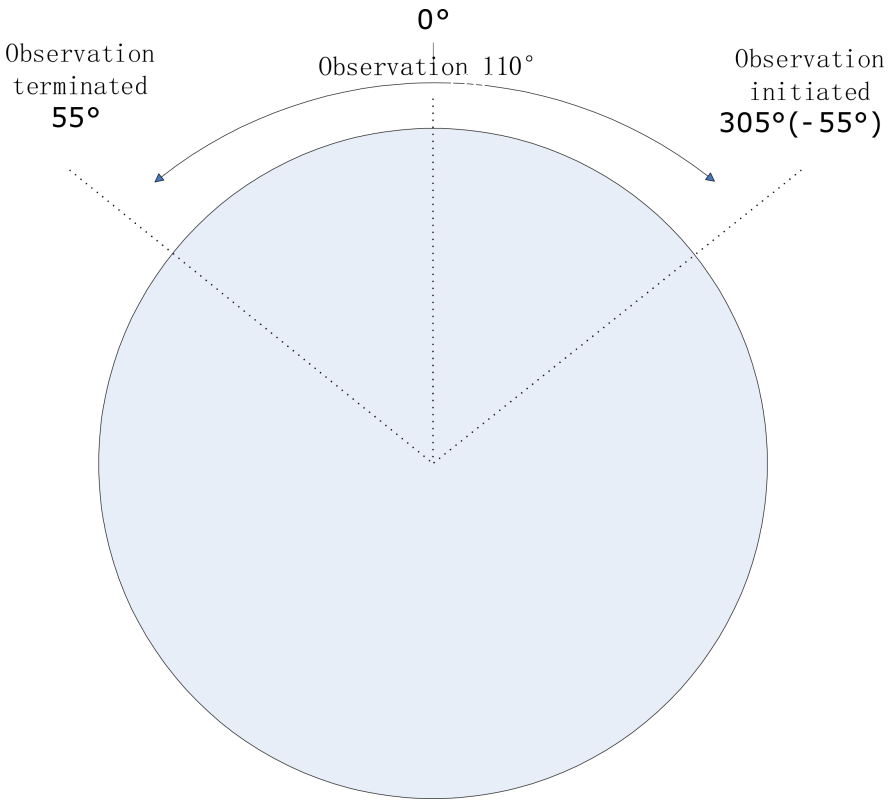

Figure 1. Antenna scanning detection.

2.2. Triple-Reflector Cassegrain Antenna

A Cassegrain antenna where the main reflector and sub-reflector are symmetric about the same axis is known as a front-fed Cassegrain antenna. In this configuration, the feed and struts create blockage effects, and the sub-reflector causes even more significant blockage, making it difficult to meet the requirement of a main beam efficiency higher than 90%. In contrast, for an offset Cassegrain antenna, both the main and sub-reflectors can be sections cut from rotationally symmetric surfaces. The axes of symmetry for the parent paraboloid and parent hyperboloid are designed not to coincide, effectively avoiding blockage of the feed by the sub-reflector [7].

The structure of the offset Cassegrain antenna is shown in **Figure 2**. Its main reflector is a rotational paraboloid, and the sub-reflector is a rotational hyperboloid. The virtual focus of the hyperboloid coincides with the real focus of the paraboloid. The feed is a rectangular or conical horn, and the phase center of the

feed is located at the real focus of the hyperboloid.

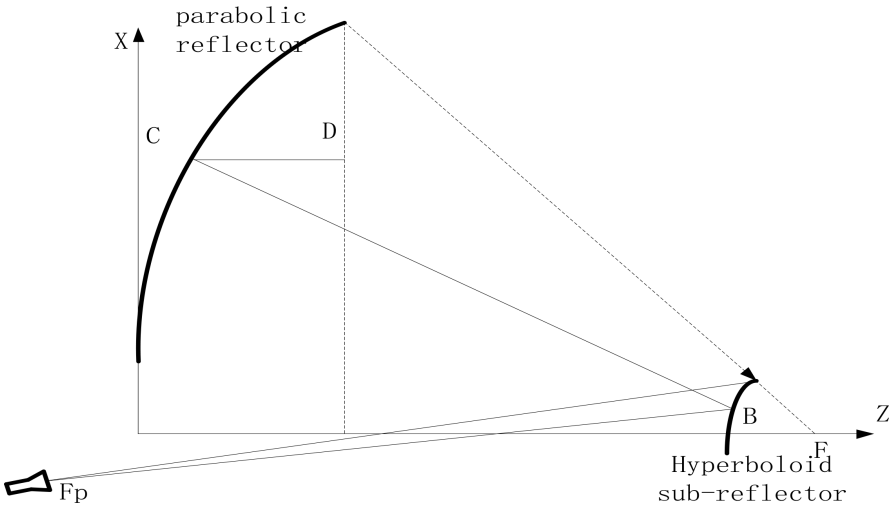

Figure 2. Offset cassegrain antenna.

The spherical electromagnetic wave emitted by the feed is reflected by point B on the hyperboloid, transforming into another spherical wave appearing to originate from the virtual focus F. After being reflected by point C on the paraboloid, it forms a plane wave and reaches point D on the aperture plane. The equation of the rotational hyperboloid in the Cartesian coordinate system is:

$$\frac{z^2}{a^2}-\frac{x^2+y^2}{b^2}=1 \tag{1}$$

where:

$$b^2=c^2-a^2 \tag{2}$$

The curvature of the hyperboloid is defined as:

$$e=\frac{c}{a} \tag{3}$$

According to the geometric properties of the hyperboloid:

$$F_pB-FB=c_1 \tag{4}$$

According to the geometric properties of the paraboloid:

$$FB+BC+CD=c_2 \tag{5}$$

Adding the equations yields:

$$F_pB+BC+CD=c_1+c_2=c_3 \tag{6}$$

In the equation, c_1, c_2, c_3 are constants. The analysis above is for an arbitrarily selected ray; the analysis for all other rays is identical. Therefore, the electromagnetic wave emitted from the feed, after reflection by the hyperboloid and paraboloid, produces an in-phase field on the aperture plane. Its advantages are as follows:

1) The Cassegrain antenna uses a paraboloid with a short focal length Fm to

achieve the performance of an equivalent paraboloid antenna with a long focal length Fe, as shown in **Figure 3**. It possesses both the structural benefits of a short focal length antenna and the electrical performance benefits of a long focal length antenna. The offset structure avoids blockage effects from the sub-reflector and feed. By replacing the main and sub-reflectors of the Cassegrain antenna with a single equivalent paraboloid, the structure is simplified into a parabolic antenna with the same feed and equal diameter, but with a focal length increased by a factor of M.

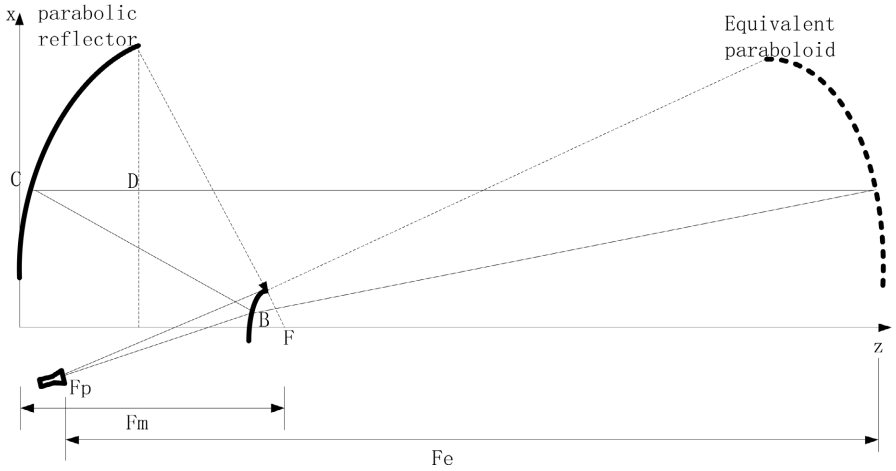

Figure 3. Eduivalent focal length of Cassegrain antenna

The relationship between the equivalent focal length and the parabolic focal length is:

$$F_e = MF_m \tag{7}$$

where the magnification factor M is:

$$M = \frac{e+1}{e-1} \tag{8}$$

2) In view of the reflector edge illumination level, a feed with a narrower beam is required. Consequently, the electromagnetic wave emitted from the feed spreads more slowly, which facilitates the design of a rotating fast-scanning mirror for local scanning.

3) The introduction of the sub-reflector adds a variable factor for controlling the illumination of the main reflector, increasing the flexibility of the antenna design.

According to the theoretical design analysis above, although the long focal length characteristic of the offset Cassegrain antenna facilitates the design of the rotating fast-scanning mirror, a Cassegrain antenna with a 5 m main reflector aperture exceeds the envelope limits of the satellite fairing. Further optimization of the antenna structure is required.

For the 5 m aperture main reflector, a folded splicing form is adopted: the central fixed section has a width of 2400 mm, and the remaining parts on both sides

utilize a folding deployment method. The feed should be located at the other virtual focus of the first sub-reflector. To facilitate compact antenna design, as well as the layout and installation of the subsequent calibration and scanning subsystems, a plane mirror is designed to mirror the virtual focus of the hyperboloid, as shown in **Figure 4**.

The upper and lower edges of the main reflector still exceed the satellite fairing envelope. The simulation of the feed illumination area on the main reflector at three observation positions (0˚ and ±55˚) is shown in **Figure 5**. The illumination levels at the upper and lower edges are relatively low, so cutting these edges has a minimal impact on the antenna's electrical performance.

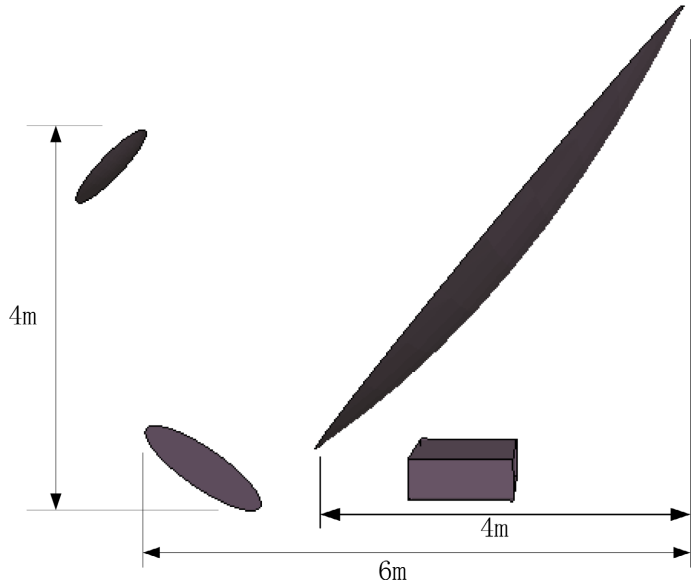

Figure 4. Triple-reflection Cassegrain antenna theory schematic.

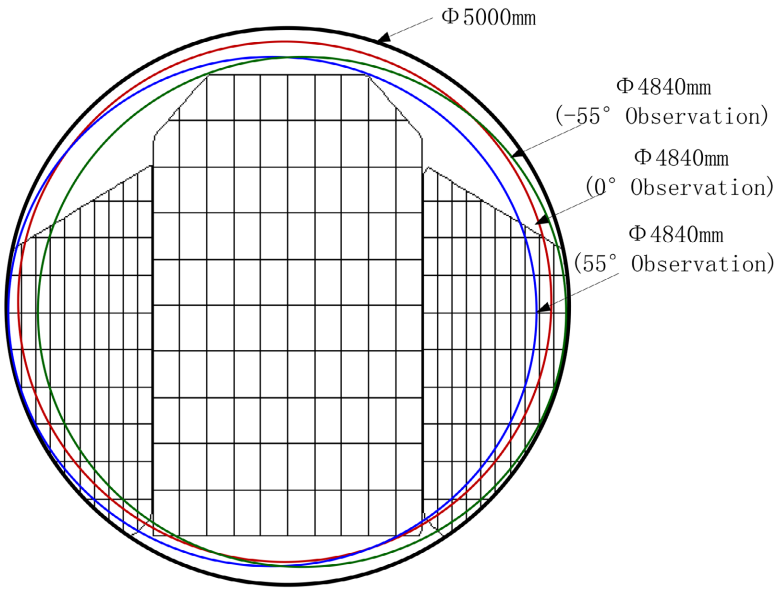

Figure 5. Illumination area of the main reflector.

Addressing the requirements of the geostationary orbit, a triple-reflector cascaded antenna system was designed. Through folding and stowing the main reflector, edge cutting, and mirroring the virtual focus of the sub-reflector, the antenna envelope size was reduced. A fast sub-scanning function is realized by a rotating scanning mirror at the feed aperture. The measured disturbance torque is 0.002 N·m, which significantly reduces the impact of disturbance torque caused by traditional mechanical scanning, while balancing system complexity and reliability requirements.

3. Simulation and Testing of Antenna Radiation Performance

The geostationary orbit microwave radiometer antenna features a 5 m aperture and operates in the sub-millimeter wave frequency bands. Collecting electromagnetic field data in the antenna's radiating near-field region and calculating far-field characteristics through mathematical transformations is the most direct and effective method for obtaining radiation parameters for large-aperture, high-frequency antenna-feed systems. Radiation performance testing serves to verify the correctness of the antenna-feed design. Simultaneously, the measured profile data of the main reflector and the geometric position data of the sub-reflectors are utilized for semi-physical simulation using the Physical Optics (PO) method in GRASP software. This validates the consistency between simulation and measurement, providing a reliable analytical method for subsequent on-orbit applications.

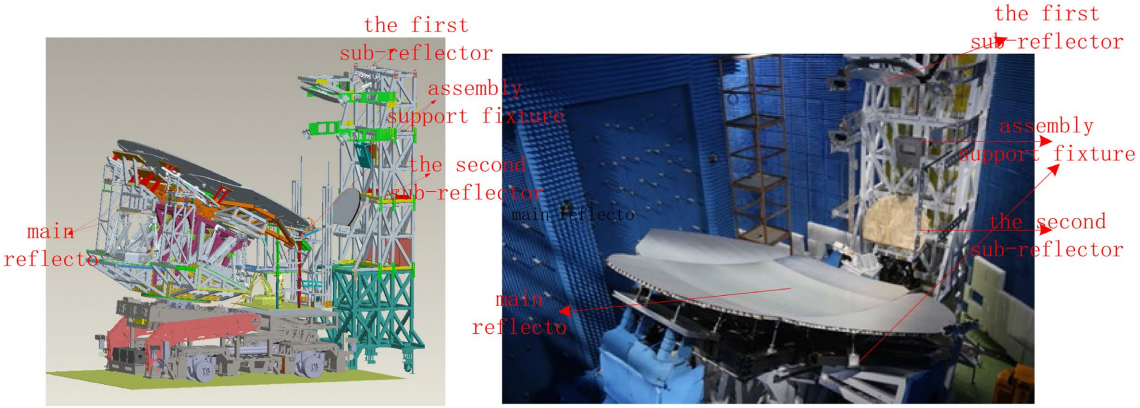

Figure 6. Model and physical object of antenna under test.

3.1. Antenna Radiation Performance Testing Method

With the central fixed section of the main reflector as the reference, the radiation performance tests are conducted using a horizontal scanning near-field test system once the left/right splicing panels of the main reflector and the first and second sub-reflectors are adjusted to their optimal states. A planar near-field scanning frame and microwave measurement system are used to capture the amplitude and phase of the probe within the antenna's near-field region. By applying a Fourier Transform to the collected near-field data, the antenna's far-field radia-

tion patterns and characteristic parameters are obtained.

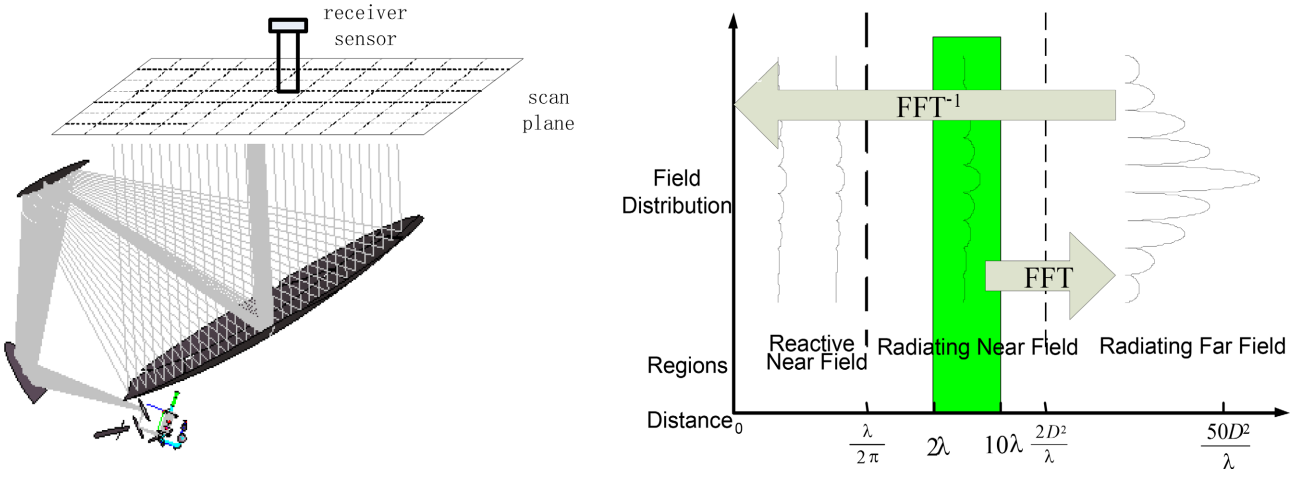

Figure 7. Planar near-field antenna test.

Antenna reflector profiles and geometric positions are measured using high-precision ground equipment. An optical point projector combined with a ground photogrammetry system is employed to acquire accuracy data for the main reflector and the two sub-reflectors. This data undergoes uniform grid interpolation. Concurrently, the attitude data of the sub-reflectors and feed components relative to the main reflector are acquired to perform semi-physical simulations and generate radiation patterns.

3.2. Semi-Physical Simulation and Testing of Antenna Patterns

The profile and geometric data of the reflector antenna measured according to the aforementioned methods are shown in **Table 2**:

Table 2. Profile and geometric measurement results.

Reflector	Spec/mm	X/mm	Y/mm	Z/mm	Spec/˚	Rx/˚	Ry/˚	Rz/˚
Sub-reflector 1	≤±0.75	−0.250	−0.139	−0.192	≤±0.01	0.0008	0.0049	−0.0050
Sub-reflector 2	≤±0.75	0.220	−0.098	−0.271	≤±0.01	−0.0015	0.0002	−0.0057
				Profile RMS/um				
Full Main Reflector				97.7				

Based on the measurement results of the profiles and geometric positions, semi-physical simulations of the antenna patterns for each frequency band were conducted, yielding main beam efficiencies better than 90%. The radiation performance was then tested using the microwave near-field scanning system. A comparative analysis between the test results and simulation data is presented in **Table 3** and **Figures 8-12**.

Comparative analysis between the semi-physical simulation and near-field

measurements demonstrates that the designed 5 m aperture offset Cassegrain antenna possesses excellent aperture distribution. Its omnidirectional main beam efficiency exceeds 90%, and sidelobe levels are better than 25 dB, achieving the

Table 3. Antenna test & simulation comparison.

Center Frequency (GHz)	54	89	118.75	165.5	183.31
Operating Bandwidth (GHz)	8	2	12	3	16
Polarization	H	V	H	V	H
Beamwidth	0.096˚	0.061˚	0.061˚	0.038˚	0.038˚
Beam Pointing	0.009˚	0.006˚	0.006˚	0.003˚	0.003˚
Main Beam Efficiency (Simulation)	94.11	94.2	94.12	93.5	92.31
Main Beam Efficiency (Measured)	93.94	93.82	93.68	92.84	91.48
Pattern Consistency (Sim vs Meas	0.17	0.38	0.44	0.66	0.83

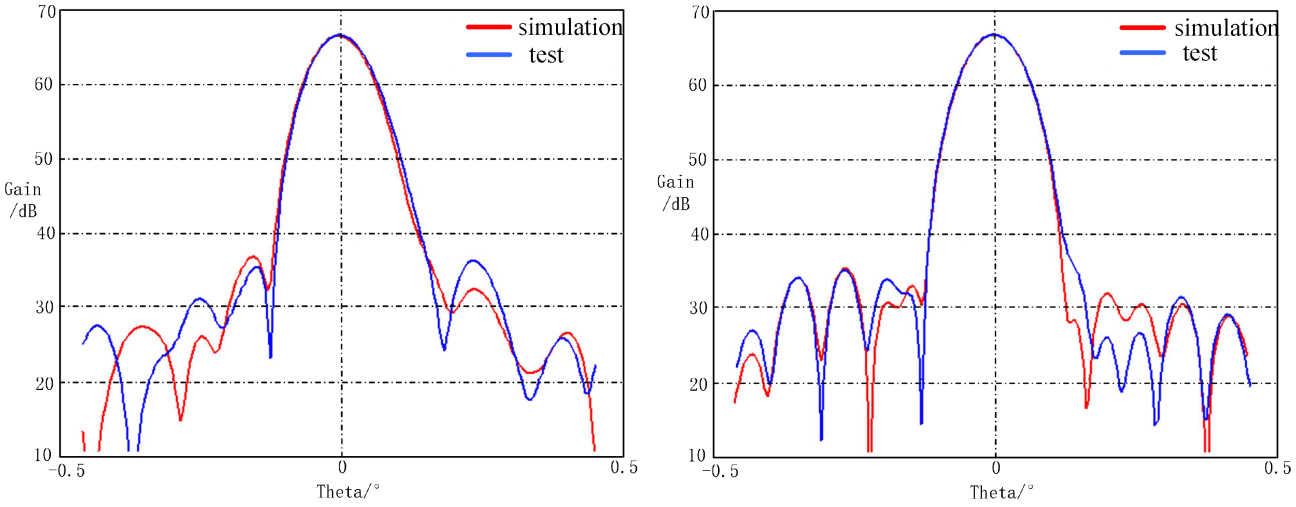

Figure 8. 54 GHz Simulated vs. measured radiation patterns (E-plane/H-plane).

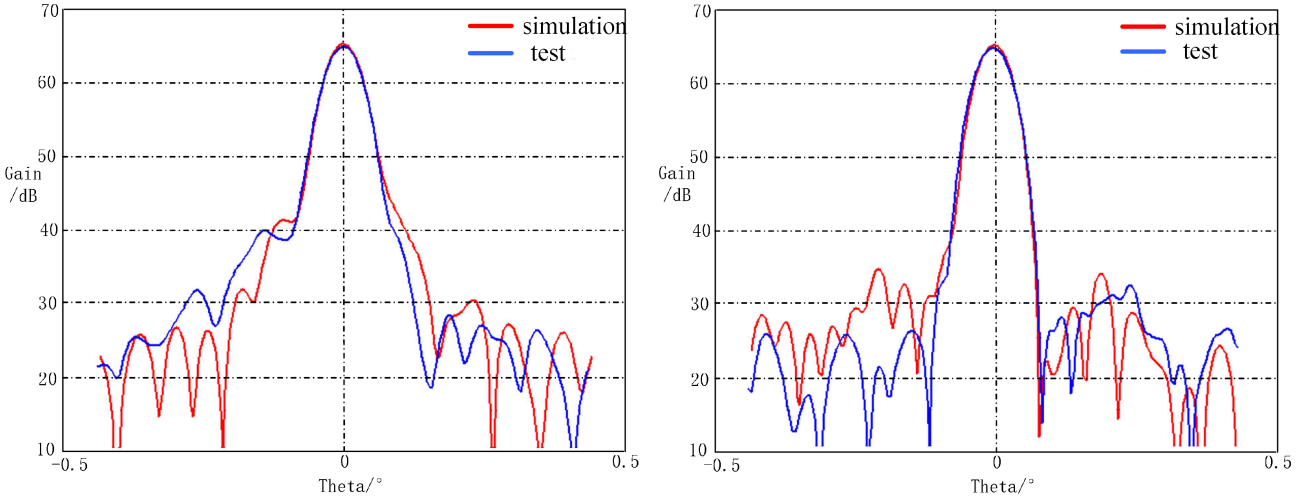

Figure 9. 89 GHz Simulated vs. measured radiation patterns (E-plane/H-plane).

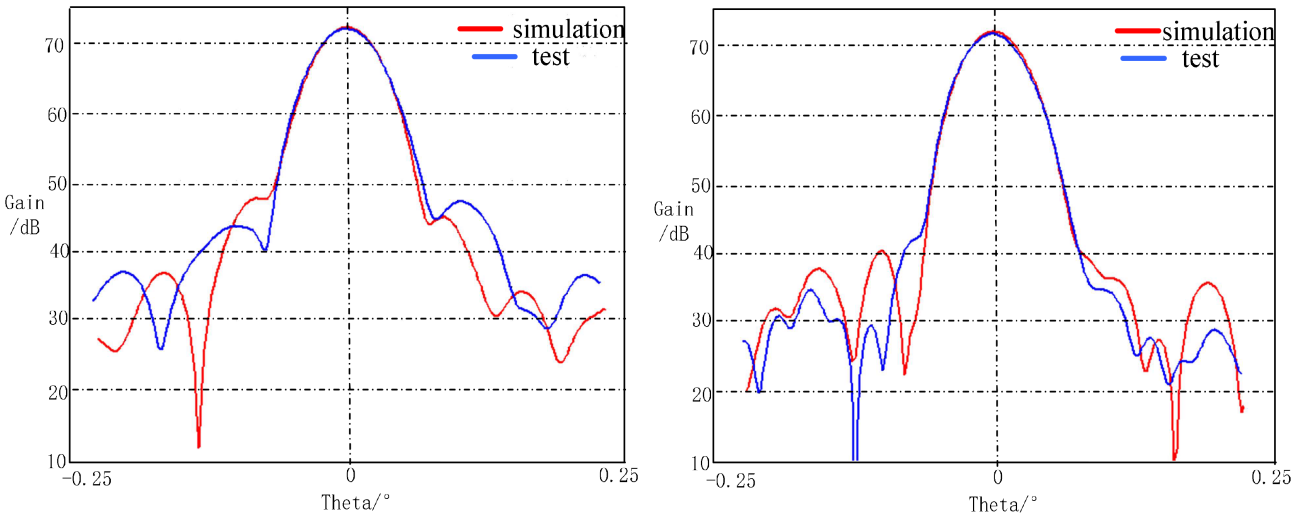

Figure 10. 118.75 GHz Simulated vs. measured radiation patterns (E-plane/H-plane).

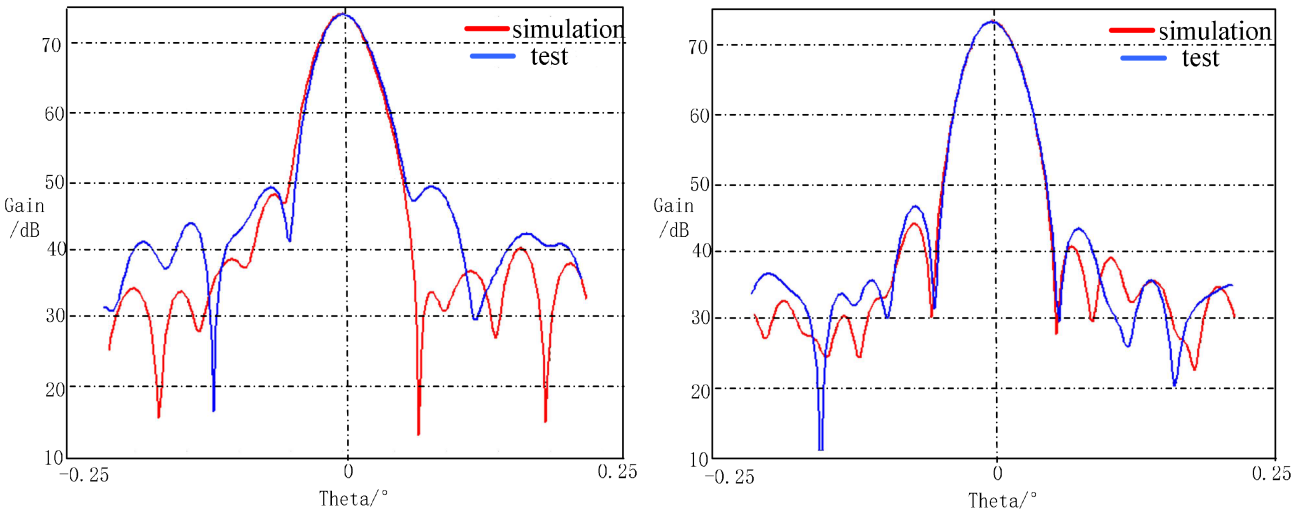

Figure 11. 165.5 GHz Simulated vs. measured radiation patterns (E-plane/H-plane).

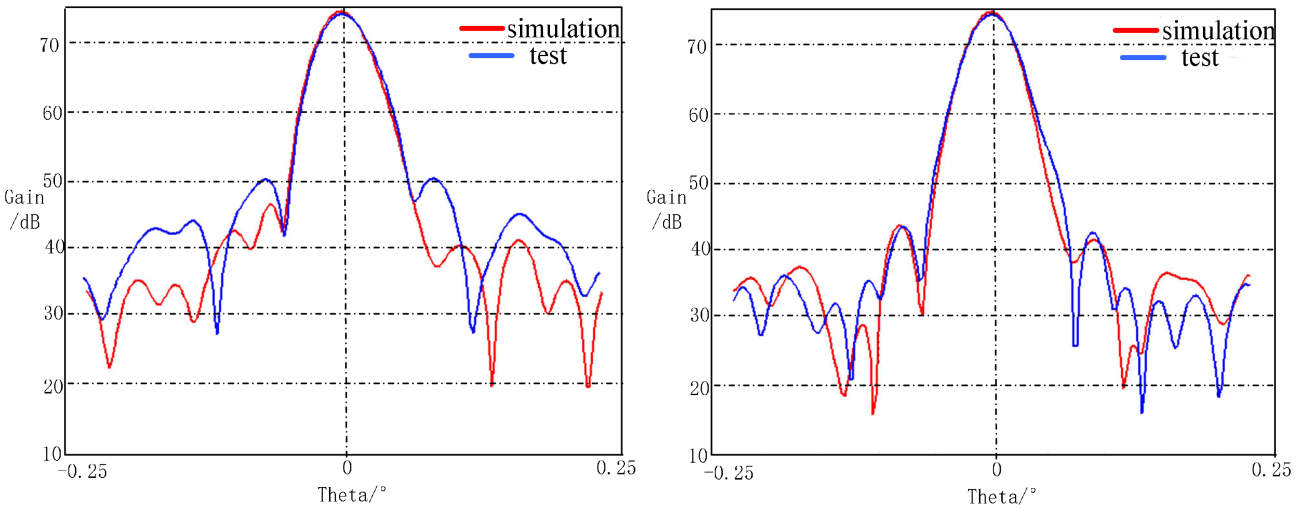

Figure 12. 183.31 GHz Simulated vs. measured radiation patterns (E-plane/H-plane).

design goals of narrow beamwidth and low sidelobes. The uncertainty of the antenna pattern between "simulation" and "measurement" is less than 1%, which is of great significance for quantitative microwave remote sensing in geostationary orbit. In the future, by conducting ground-based simulation analysis using on-orbit measurement data of the antenna profile and geometry, the error caused by pattern uncertainty will be minimized, ensuring the detection accuracy of microwave remote sensing.

4. Conclusion

In the field of meteorology, microwave sounding from geostationary orbit has long been constrained by factors such as spatial resolution and calibration accuracy. Consequently, while international agencies have conducted pre-research and exploration, none have yet moved forward with substantial engineering development. China has taken the lead in the development of geostationary microwave sounding satellites. By utilizing a folding-and-splicing design for the large-aperture antenna combined with a focal imaging configuration, the satellite's envelope requirements have been successfully met. The simulation and experimental validation of the antenna-feed system provide a reliable analytical methodology for its operation in orbit. In the future, geostationary microwave sounding satellites will fill the gap in high-frequency atmospheric profiling of cloudy and rainy regions. This will significantly enhance forecasting and early warning capabilities for extreme weather events, such as strong convection and typhoons, marking a major milestone in the development of meteorological satellites for China and the global community.

Conflicts of Interest

The authors declare no conflicts of interest regarding the publication of this paper.

References

[1] Qian, B., Cao, A.J., Wu, Y., *et al.* (2017) A Review on Geostationary Earth Orbit Microwave Atmospheric Sounding Technology. *Remote Sensing for Land and Resources*, **29**, 1-5.

[2] Lu, N.M. and Gu, S.Y. (2016) The Status and Prospects of Atmospheric Microwave Sounding by Geostationary Meteorological Satellite. *Advances in Met S&T*, **6**, 120-123.

[3] Chen, K., Zheng, Z.M., *et al.* (2021) Performance of Geostationary Orbit Millimeter-Wave Atmospheric Soundings Based on End to End Simulations. *Journal of Infrared and Millimeter Waves*, **40**, 1001-9014.

[4] Xie, Z.C., Xu, H.X., An, D.W., *et al.* (2018) Remote Sensing Technology of Experimental Microwave Radiometer in Geostationary Orbit. *Aerospace Shanghai*, **35**, 49-58.

[5] Yu, X.J., Li, J.Y. and Zhang, X.G. (2019) Beam Scanning Characteristics of Side-Feed Offset Cassegrain Antenna. *Chinese of Radio Science*, **34**, 628-632.

[6] Ulaby, F.T., Moore, R.K. and Fung, A.K. (1988) Microwave Remote Sensing. Beijing Science Press, 13-37.

[7] Chen, X., Qu, J., Yu, C., *et al.* (2012) The Shaped Millimeter-Wave Antenna with Offset Feed and Dual-Reflector. *Journal of Infrared and Millimeter Waves*, **31**, 42-46.